Pergamon

Int. J. Multiphase Flow Vol. 24, No. 1, pp. 77–92, 1998

Printed in Great Britain
PII: S0301-9322(97)00042-6
0301-9322/98 $19.00 + 0.00

DIRECT SIMULATION OF CHARGED PARTICLE DEPOSITION IN A TURBULENT FLOW

M. SOLTANI,[1] G. AHMADI,[1] H. OUNIS[1] and J. B. McLAUGHLIN[2]

[1]Department of Mechanical and Aeronautical Engineering, Clarkson University, Potsdam, NY 13699, U.S.A. [2]Department of Chemical Engineering, Clarkson University, Potsdam, NY 13699, U.S.A.

(Received 15 April 1996; in revised form 22 May 1997)

Abstract—Wall deposition of charged particles in a turbulent duct flow in the presence of electrostatic charges is studied. The turbulent flow velocity field is generated by a direct numerical simulation of the Navier–Stokes equation via a pseudospectral method. It is assumed that the particles are sufficiently small and widely separated that they do not interact and have no influence on the fluid motion.

The equation of motion of particles including the Brownian and electrostatic forces is used in the analysis. Ensembles of 8192 charged particle trajectories are evaluated and statistically analyzed. Uniform and Boltzmann charge distributions on the particles are considered. Effects of size and electric field intensity on particle dispersion and wall deposition rate are studied. The results are compared with those obtained from empirical equations. © 1997 Elsevier Science Ltd

Key Words: charged particle deposition, turbulent flow, direct simulation

1. INTRODUCTION

Aerosol dispersion and deposition play a major role in many natural phenomena, as well as in various industrial applications. Coal transport and cleaning, micro-contamination control, and xerographic processes are a few examples. In many cases, the charges carried by particles affect their deposition. The particle deposition process with electrostatic forces was studied by several researchers in the past three decades. Yu and Chandra (1978) analyzed the precipitation of charged particles by their image forces from laminar flows in ducts with different geometries. Using an integral method, the deposition of contaminant particles from a laminar flow in the presence of electrostatic forces was studied by Chen (1978a, b). Cooper *et al.* (1989) analyzed the deposition rates of submicrometer particles due to diffusion and electrostatics in a viscous axisymmetric stagnation-point flow. Ahmadi (1972) studied the diffusion of charged Brownian particles in the presence of electromagnetic fields. A digital simulation technique for studying deposition rates of aerosol particles with electrostatic forces was reported by Li and Ahmadi (1993a). Soldati *et al.* (1993) used a direct numerical simulation to study the particle transport in electrostatic precipitators.

Use of digital simulation techniques for studying dispersion of small particles in turbulent flows was the subject of a number of papers. Turbulent dispersion of small particles was studied by Ahmadi and Goldschmidt (1971). Ounis and Ahmadi (1990b) considered the combined effects of turbulence and Brownian motion on the dispersion of small aerosol particles. McLaughlin (1989) and Ounis *et al.* (1991a, 1993), Squire and Eaton (1991), and Brooke *et al.* (1992) analyzed the aerosol particle deposition in a channel where the instantaneous turbulent flow field was simulated using a pseudospectral computer code. Recent developments in the direct numerical simulation were reviewed by McLaughlin (1994). Brownian diffusion of submicron particles in the viscous sublayer was studied by Ounis *et al.* (1991b). Abuzeid *et al.* (1991) analyzed the dispersion and deposition processes of particles released from point sources in turbulent channel flow. Li and Ahmadi (1992, 1993b) simulated the deposition rate of aerosols in turbulent channel flows near smooth and rough walls. A computational procedure for analyzing particle transport and

deposition in complex passages was described by Li *et al.* (1994). However, the details of the interaction of charged particles and turbulent near wall flows are not fully understood.

In this study, a direct numerical simulation procedure for studying the deposition and diffusion processes of charged aerosol particles in a turbulent channel flow field in the presence of electrostatic forces is described. The particle equation of motion that includes the Brownian diffusion, the Coulomb and the image forces is used. Starting with an initially uniform concentration near the wall, deposition velocities of charged particles with uniform and Boltzmann equilibrium distribution are evaluated. An ensemble of 8192 particles and several electric field strengths is used in this simulation. The results are compared with those obtained from empirical equations and good agreement is observed.

2. TURBULENT FLOW FIELD

The velocity field in the channel must first be simulated in order to solve the particle equation of motion. To generate the instantaneous turbulent velocity field components, the Navier–Stokes and mass conservation equations are numerically solved. The corresponding governing equations are

$$\nabla \cdot \mathbf{v}^{\mathrm{f}} = 0$$

$$\frac{\partial \mathbf{v}^{\mathrm{f}}}{\partial t} + \mathbf{v}^{\mathrm{f}} \cdot \nabla \mathbf{v}^{\mathrm{f}} = -\frac{1}{\rho} \nabla p + \nu \nabla^2 \mathbf{v}^{\mathrm{f}} \qquad [1]$$

where $\mathbf{v}^{\mathrm{f}}$ is the fluid velocity, p is the pressure, ν is the viscosity and ρ is the mass density. Note that in [1] the flow is assumed to be incompressible and is driven by a constant pressure gradient. In order to solve [1], the no-slip boundary conditions on the wall are used, i.e.

$$\mathbf{v}^{\mathrm{f}} = 0 \quad \text{at} \quad y = \pm h/2 \qquad [2]$$

where h denotes the channel width. All quantities are nondimensionalized with the aid of wall units. Using the friction velocity u^* and the kinematic viscosity ν, the wall units of length and time are, respectively, given by ν/u^* and ν/u^{*2}.

The computational method used to solve the Navier–Stokes equation was developed by Azab and McLaughlin (1987). To account for the nonlinear term, the pressure and the viscous terms, three fractional time steps are used to solve the fluid velocity from time step (N) to time step ($N + 1$). Additional details of the numerical simulation technique were described by McLaughlin (1989). The required computational resolution of the direct simulation increases rapidly with increasing Reynolds number. Therefore, due to computational time limitations, a low Reynolds number turbulent channel flow field is considered in this study. The Reynolds number based on the hydraulic diameter of the channel and the mean velocity is approximately 7050. The channel considered has a height h of 250 wall units between the two parallel walls. Periodic cells of 630 wall units in both spanwise (z-direction) and streamwise (x-direction) were considered. Respectively, 16, 65 and 64 computational grid points in the x, y and z directions were used. The collocation points in the y direction were computed using Chebyshev series, while the grid points in the x direction were equally spaced.

The velocity field across the channel in one periodic cell at $t^+ = 100$ and streamwise location of $x^+ = 236.25$ is shown in figure 1(a). While the field in the yz plane is random, certain coherent structures and flow patterns pointing towards and away from the wall are clearly observed in this figure. The velocity vector field at $t^+ = 100$ in the xz plane at a distance of $Y_0^+ = 1.3$ ($Y_0^+ = 125 - y^+$) wall units away from the upper channel wall is shown in figure 1(b). While the flow is predominantly in the x direction, the low and high speed streaks can clearly be seen in the figure.

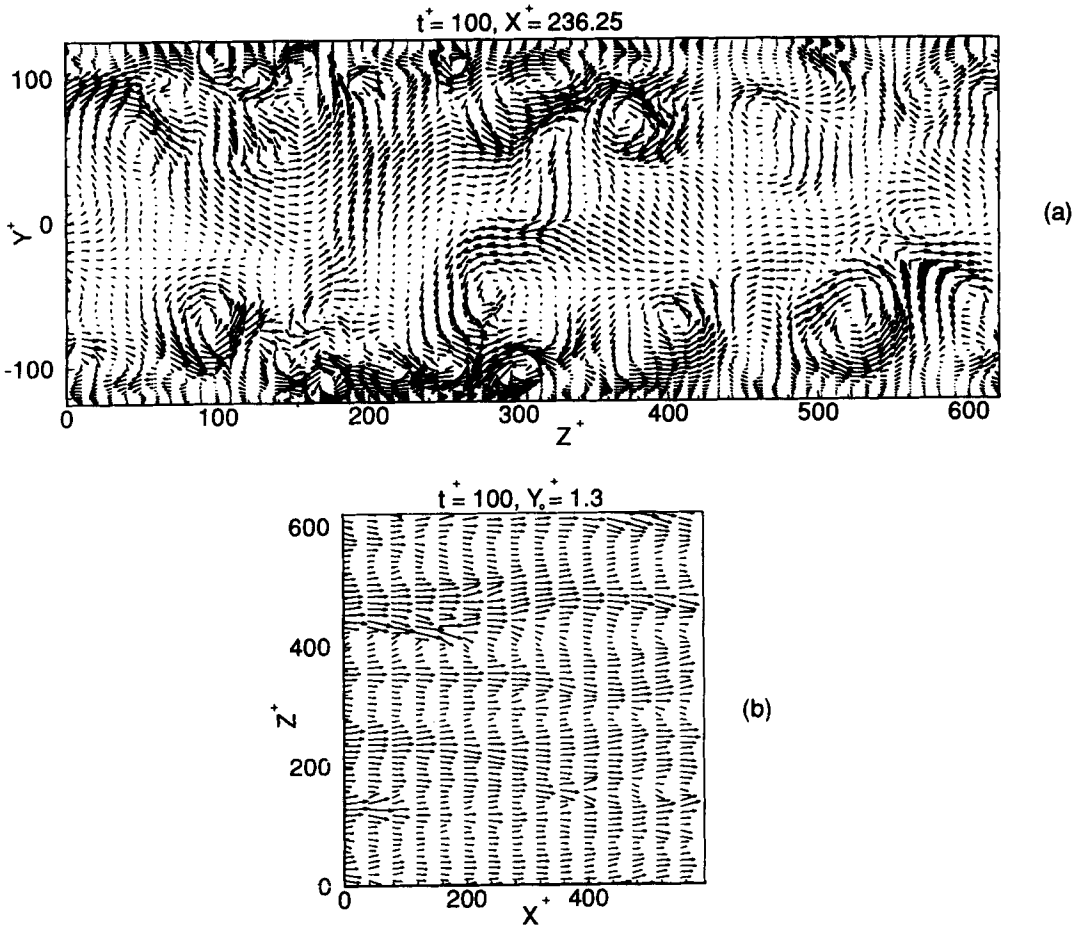

Figure 1. Instantaneous velocity vector plots at $t^+ = 100$: (a) yz plane; (b) $Y_0^+ = 1.3$ plane.

3. EQUATION OF PARTICLE MOTION

The equation of motion of a charged aerosol particle including the Brownian and electrostatic forces is given by

$$\frac{dv_i^p}{dt} = \frac{18\nu}{d^2 SC_c}(1 + 0.15\mathrm{Re}^{0.687})(v_i^f - v_i^p) + \frac{2K\nu^{1/2}d_{ij}}{Sd(d_{ik}d_{kl})^{1/4}}(v_j^f - v_j^p) + \frac{N_i(t)}{m} + \frac{F_e}{m} \qquad [3]$$

Table 1. Neutral fraction, average absolute charge for various particle diameters

Diameter (μm)	τ_p^+/C_c	Neutral fraction $f(0)$	Absolute charge number
0.01	2.4×10^{-8}	0.993	0.007
0.02	9.64×10^{-8}	0.892	0.10
0.03	2.17×10^{-7}	0.781	0.23
0.05	6×10^{-7}	0.606	0.53
0.1	2.4×10^{-6}	0.428	0.75
0.5	6×10^{-5}	0.191	1.67
1	2.4×10^{-4}	0.135	2.36
2	6×10^{-3}	0.0957	3.34
3	2.16×10^{-3}	0.0782	4.09
5	6×10^{-3}	0.0606	5.28
10	2.4×10^{-2}	0.0428	7.46
200	9.64	0.0095	33.37
300	21.69	0.0078	40.87

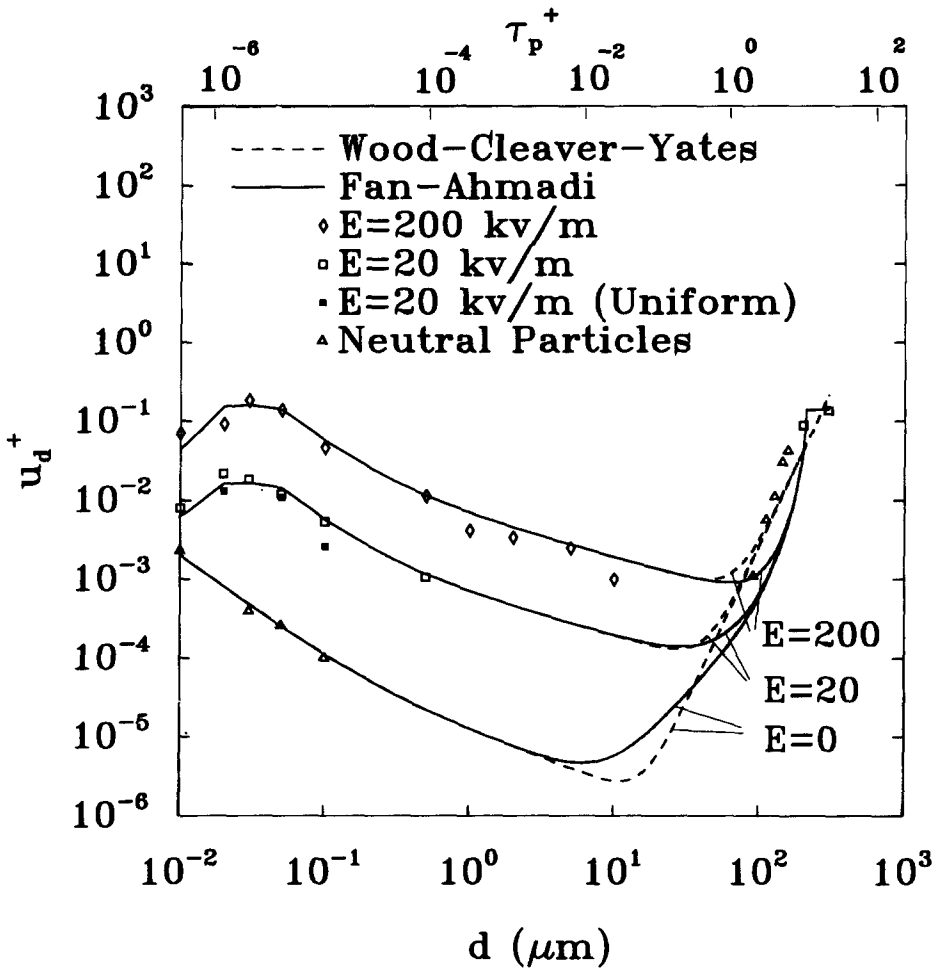

Figure 2. Variation of particle deposition velocity with diameter and particle relaxation time for different applied electric fields.

and

$$\frac{dx_i}{dt} = v_i^p \qquad [4]$$

where v_i^p is the velocity of the particle, v_i^f is the instantaneous fluid velocity, x_i is its position, t is the time, d is the particle diameter, $S = \rho^p/\rho^f$ is the ratio of particle density ρ^p to fluid density ρ^f, m is the mass of the particle, $K = 2.594$ is the constant coefficient of the Saffman (1968) lift force, $N_i(t)$ is the Brownian force per unit mass, F_e is the electrical force. In [3], $\mathrm{Re} = |\mathbf{v}^f - \mathbf{v}^p|d/v$ is the particle Reynolds number based on the particle velocity relative to the fluid, and the fluid kinematic viscosity v, and C_c is the Stokes–Cunningham slip correction factor given as

$$C_c = 1 + \frac{2\lambda}{d}(1.257 + 0.4e^{-1.1d/2\lambda}) \qquad [5]$$

where λ is the molecular mean free path of the gas and the deformation rate tensor d_{ij} is defined as

$$d_{ij} = \frac{1}{2}\left(\frac{\partial u_i}{\partial x_j} + \frac{\partial u_j}{\partial x_i}\right). \qquad [6]$$

The first term on the right-hand side of [3] is the drag force caused by the relative motion between particles and fluid. Here, to account for the nonlinear variation of drag, an empirical equation

suggested by Clift *et al.* (1978) is used. The second term is the Saffman lift force. The third term is the Brownian force due to molecular agitation, and the last term is the electrical force which includes the Coulomb and the image forces. Ounis and Ahmadi (1989, 1990a) showed that the virtual mass, the Faxen correction, Basset history effects, and pressure forces have little effect on the diffusion of small particles considered in this analysis. Hence, these forces are not included in [3].

It should be noted that the wall effect is not included in the expressions for drag and lift forces in [3]. In addition, the effect of van der Waals attraction is also ignored. Therefore, this equation is not strictly accurate when the distance of the particle from the wall is small (smaller than the particle size). However, the increase of the drag force when a particle approaches the wall is of comparable order to the surface attractive forces. Therefore, neglecting these opposite effects will not alter the results to an appreciable extent. The gravitational sedimentation effect is also neglected in the present study. Thus, the simulation results are for particles that are moving in a vertical channel flow. Furthermore, the present study is concerned with highly dilute flows, for which the effects of particles on modifying the turbulent flow field, as well as particle–particle interactions, are negligible.

4. DIMENSIONLESS PARTICLE EQUATION OF MOTION

Using the wall units, [3] may be restated in nondimensional form as

$$\frac{dv_i^{+p}}{dt^+} + \frac{1}{\tau_p^+}(1 + 0.15\mathrm{Re}^{0.687})v_i^{+p} = \frac{1}{\tau_p^+}(1 + 0.15\mathrm{Re}^{0.687})v_i^{+f} + \frac{2Kd_{ij}^+}{Sd^+(d_{ik}^+ d_{kl}^+)^{1/4}}(v_j^{+f} - v_j^{+p}) + n_i^+(t^+) + F_e^+ \quad [7]$$

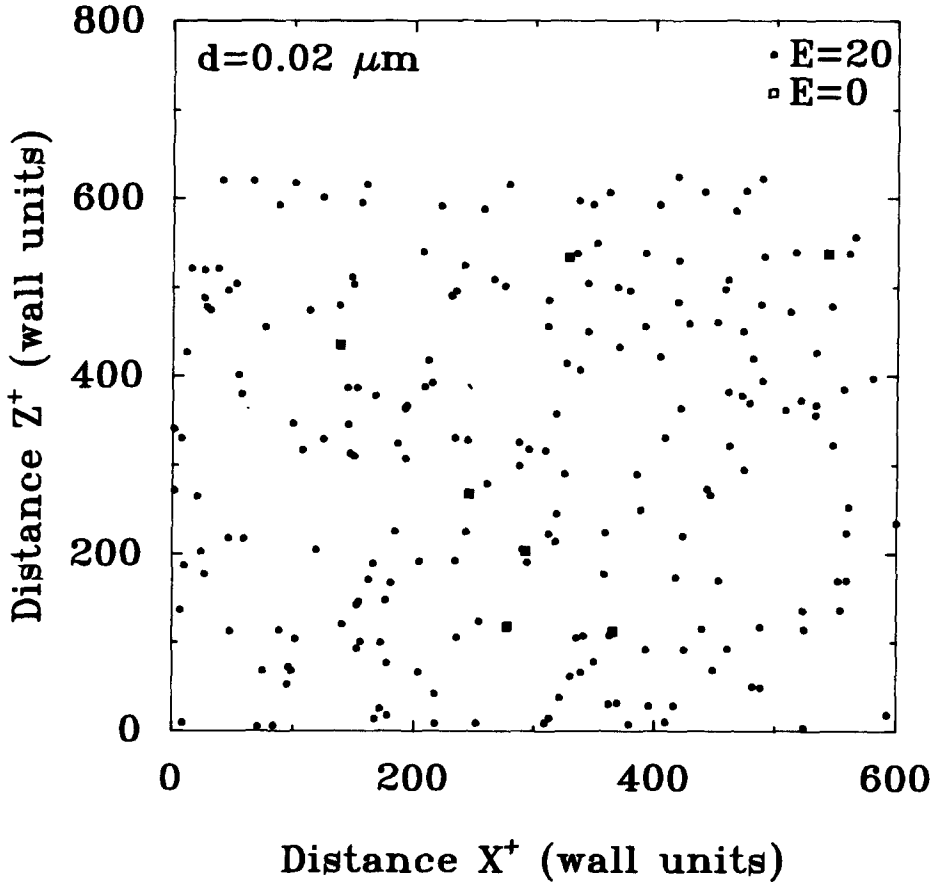

Figure 3. Distribution of the initial locations of the deposited particles in the xz plane.

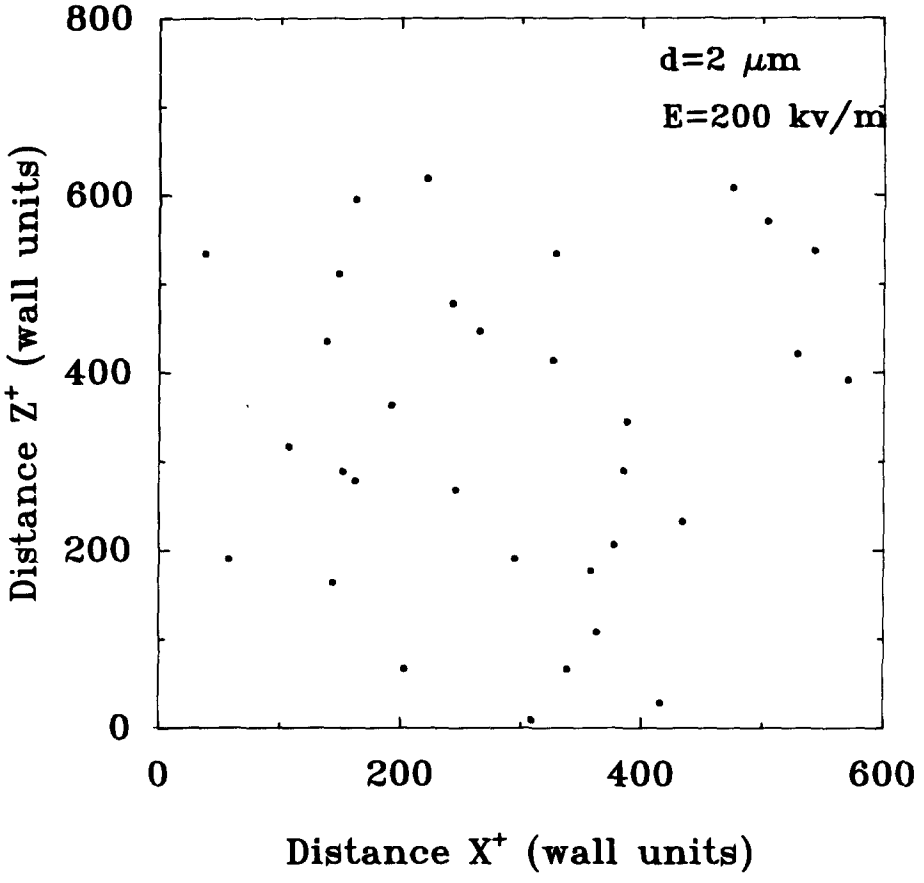

Figure 4. Distribution of the initial locations of the deposited particles in the xz plane.

where

$$x^+ = \frac{xu^*}{\nu}, \quad v_i^+ = \frac{v_i}{u^*}, \quad t^+ = \frac{tu^{*2}}{\nu}, \quad d_{ij}^+ = \frac{d_{ij}\nu}{u^{*2}}. \tag{8}$$

Here v_i^{+p} and v_i^{+f} denote the nondimensional particle and fluid velocities, respectively, u^* is the shear velocity, n_i^+ is the nondimensional Brownian excitation, τ_p^+ is the dimensionless particle relaxation time (Stokes number) defined as

$$\tau_p^+ = \tfrac{1}{18} C_c S d^{+2} \tag{9}$$

where the dimensionless particle diameter, d^+, is given by

$$d^+ = \frac{du^*}{\nu}. \tag{10}$$

Note that the Cunningham correction factor C_c is included in the definition of τ_p^+, as given by [5].

In [7], the nondimensional Brownian force n_i^+ and the nondimensional electrostatic force F_e^+ are given as

$$n_i^+(t^+) = \frac{6\nu}{\pi \rho^p d^3 u^{*3}} N_i(t^+), \quad F_e^+ = \frac{6}{\pi S d^{+3} \rho^f \nu^2} F_e. \tag{11}$$

The spectral intensity of n_i^+ is given by

$$S_{n_i^+ n_j^+}(\omega^+) = \frac{216}{\pi^2 C_c} \left(\frac{kT}{\mu \nu d}\right) \frac{1}{S^2 d^{+4}} \delta_{ij} \tag{12}$$

where ω^+ is the frequency in wall units, T is the temperature of the gas, $k = 1.38 \times 10^{-23}$ J/K is the Boltzmann constant, and μ is the coefficient of viscosity. [12] may be restated as

$$S_{n_i^+ n_j^+}(\omega^+) = \frac{648}{\pi C_c^2} \frac{\delta_{ij}}{S_c S^2 d^{+4}} = \frac{2}{\pi S_c \tau_p^{+2}} \delta_{ij} \qquad [13]$$

where

$$S_c = \frac{\nu}{D} = \frac{3\pi \nu d \mu}{C_c k T} \qquad [14]$$

is the Schmidt number and D is the Brownian diffusivity. The intensity of the dimensionless Brownian force increases rapidly as the particle diameter decreases. This increase is due to the fact that the spectral intensity of N_i varies with $(1/d^5)$ as shown by [12]. The explicit expression for the electrostatic force is described in the following section.

For evaluating the drag and the lift forces in [7], the instantaneous fluid velocity at the particle mass center is needed. Here, partial Hermite interpolation is used to obtain the streamwise and spanwise fluid velocity components at the particle location, while a direct spectral sum is used for the direction normal to the walls. Additional details of simulation procedure were described by McLaughlin (1989, 1994) and Ounis *et al.* (1991a).

5. ELECTROSTATIC FORCE

The total electric charge on a particle that carries n units of charge is given by

$$q = ne \qquad [15]$$

where $e = 1.6 \times 10^{-19}$ C is the electric unit charge. The force acting on a charged particle suspended in a gas near a conducting surface is given as (Hartmann *et al.* 1976; Cooper *et al.* 1989; Li and Ahmadi 1993a)

$$F_e = qE - \frac{q^2}{16\pi\epsilon_0 y^2} + \frac{qEd^3}{16y^3} - \frac{3}{128} \frac{\pi \epsilon_0 d^6 E^2}{y^4} \qquad [16]$$

where $\epsilon_0 = 8.859 \times 10^{-12}$ A s/V m is the permittivity, E is the electric field strength, and y is the distance of the particle from the wall. In [16], the first term on the right-hand side is the Coulomb force due to the passage of an electric field. The second term is the image force exerted by an image charge of $-q$ at position $-y$ from the surface. The third term is the dielectrophoretic force on the induced dipole caused by the gradient of the field from the image charge. The last term in [16] is the dipole–dipole force effect. The Coulomb and dielectrophoretic forces can be either toward or away from the wall. While the image force is always directed towards the surface. When an external electric field is present, Li and Ahmadi (1993a) showed that the Coulomb force dominates. In this analysis, therefore, only Coulomb and image forces are included and the other terms, which are generally small, are neglected. In general, the image force is also quite short range, so that its effect on the particle deposition process is insignificant.

6. UNIFORM AND BOLTZMANN CHARGE DISTRIBUTION

Natural as well as man made aerosol particles are usually electrically charged. Small particles in a bipolar ionic atmosphere tend toward the Boltzmann charge distribution (Fuchs 1964; Hidy 1984). Thus, under equilibrium conditions, the fraction $f(n)$ of particles of diameter d with n elementary electronic charges is given by

$$f(n) = \frac{e^{-n^2 e^2/dkT}}{\sum_{n=-\infty}^{\infty} e^{-n^2 e^2/dkT}} \qquad [17]$$

where k is the Boltzmann constant, e is the electronic unit of charge, and T is the temperature. For particles larger than 0.03 μm, [17] may be approximated by a Gaussian distribution (Cooper *et al.* 1989), i.e.

$$f(n) = \sqrt{\frac{e^2}{\pi dkT}}\, e^{-n^2e^2/dkT}, \quad \text{for} \quad d \geqslant 0.03\ \mu\text{m}. \tag{18}$$

The average number of absolute charges per particle is given as

$$\overline{|n|} = \sum_{n=0}^{\infty} |n| f(|n|). \tag{19}$$

For large particles, the summation in [19] may be approximated by an integral, i.e.

$$\overline{|n|} \simeq \sqrt{\frac{dkT}{\pi e^2}}, \quad \text{for} \quad d \geqslant 0.03\ \mu\text{m}. \tag{20}$$

[20] gives the average number of absolute charges per particle for d greater than 0.03 μm. Therefore, $|n|/2$ is the number of positive or negative charges carried by a particle. For particles smaller than 0.03 μm, the summation in [20] has to be evaluated numerically. Using the exact distribution function, the results for the uncharged fraction and the mean absolute charge values are listed in table 1. These values are used in the present simulation.

Under ideal conditions, where aerosols have the same probability of encountering positive or negative ions, the Boltzmann charge distribution is a reasonable assumption. However, the real

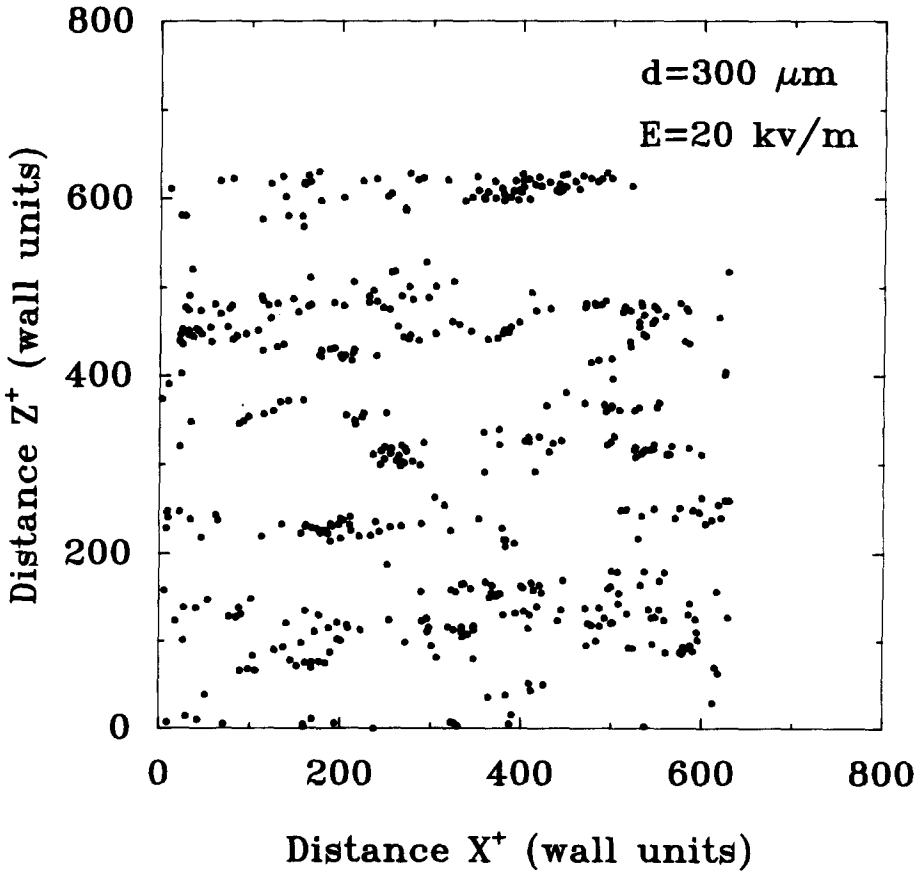

Figure 5. Distribution of the initial locations of the deposited particles in the xz plane.

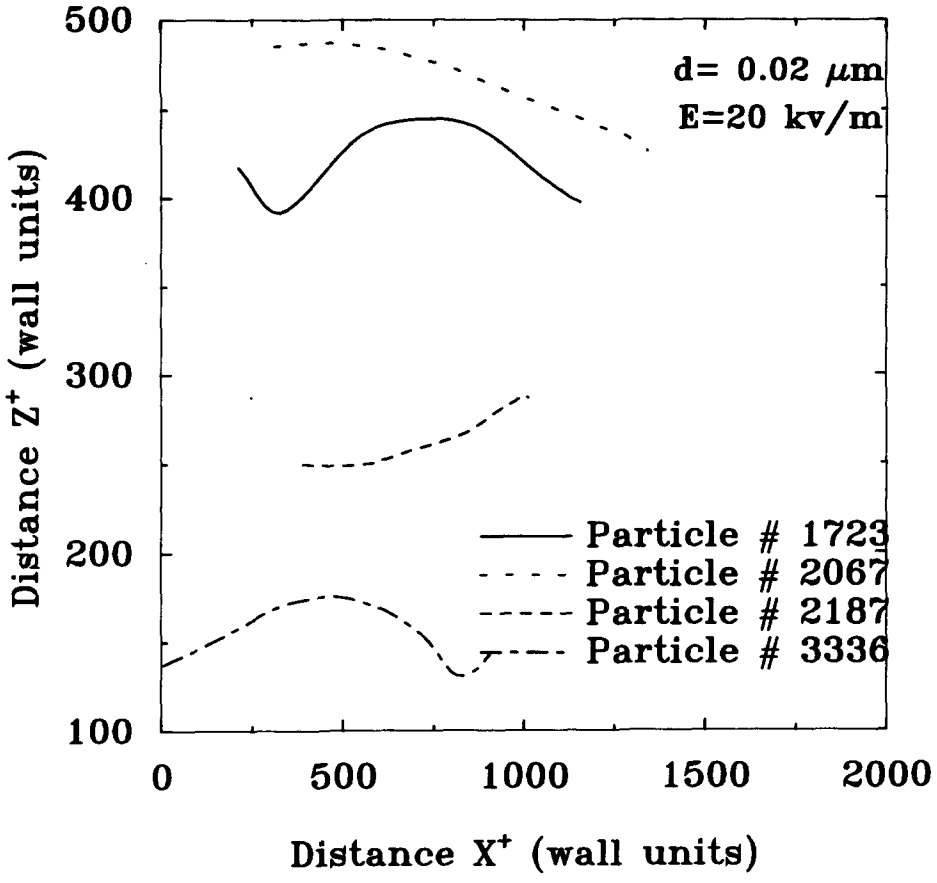

Figure 6. Sample particle trajectories in the xz plane.

charge distribution, especially in the presence of an electric field, may be quite different. Adachi *et al.* (1985) and Porstendorfer *et al.* (1984) studied the charge distributions in the atmosphere and noted that it differs from the Boltzmann distribution for particles less than 0.1 μm. The difference is due to the fact that, in general, the negative ions tend to have higher mobility and diffusivity when compared with the positive ions. As a result, the distribution for small particles is skewed towards negative number of charges.

In spite of its shortcomings, the Boltzmann distribution is used in the subsequent analysis as a first approximation. However, the simulation methodology is applicable to any other reasonable charge distribution for small particles.

[7] together with [11] and [16] are used for the Lagrangian Brownian Dynamic (BD) simulation of charged particle trajectories. The details of the particle trajectory analysis procedure in the absence of electrical effects were described by Ounis *et al.* (1991a, b).

7. EMPIRICAL MODELS

Due to the absence of controlled experimental data concerning charged particle deposition rate in turbulent flows, empirical equations are used to compare the results of the present simulation. Fan and Ahmadi (1994) showed that the superposition (linear addition) of various effects is a reasonable approximation for estimating the deposition rates of charged particles. Using a sublayer model, Cleaver and Yates (1975) developed an expression for the Brownian particle deposition rate. Adding to their expression the contribution of eddy-impaction effects suggested by Wood (1981) and the electrostatic precipitation rate, it follows that

$$u_d^+ = 0.085\mathrm{Sc}^{-2/3} + 4.5 \times 10^{-4}\tau_p^{+2} + \frac{\bar{q}ED}{2kTu^*} \qquad [21]$$

where $\bar{q} = \overline{|n|}e$ is the absolute average charge, D is the diffusivity coefficient and Sc is the Schmidt number. The first term in [21] is particle deposition due to Brownian motion and eddy diffusion. The second term is particle deposition induced by eddy diffusion-impaction. The third term is the electrostatic sedimentation velocity due to the Coulomb force in the presence of an applied electric field.

Recently, Fan and Ahmadi (1993) developed an empirical equation for deposition of particles on smooth and rough surfaces in turbulent flows. In the absence of gravitational effects and for smooth walls, the model reduces to

$$u_d^+ = 0.084\mathrm{Sc}^{-2/3} + 0.0185\left[\frac{1 + 8e^{-(\tau_p^+ - 10)^2/32}}{1 - 3.08\tau_p^{+2}/(Sd^+)}\right]\left[\frac{d^{+2}}{13.68}\right]^{1/[1 + 3.08\tau_p^{+2}/(Sd^+)]} + \frac{\bar{q}ED}{2kTu^*} \qquad [22]$$

where the electrostatic sedimentation velocity is added linearly to [22].

[21] and [22] are used in the next section for comparison with the present simulation results for particle deposition rate.

8. RESULTS AND DISCUSSION

In this section, digital simulation results for dispersion and deposition rate of aerosol particles in the presence of electrostatic charges are described. The air is assumed to be at 297 K with a kinematic viscosity of $\nu = 1.5 \times 10^{-5}$ m^2/s and a density of $\rho = 1.12$ kg/m^3. A friction velocity of 3.7 cm/s, which is a common value for clean room applications, is also assumed. Under this condition, one wall unit of length (ν/u^*) is about 405 μm, and the corresponding wall unit of time (ν/u^{*2}) is 0.011 s. A density ratio of $S = 713$ and different particle diameters ranging from 0.01 to

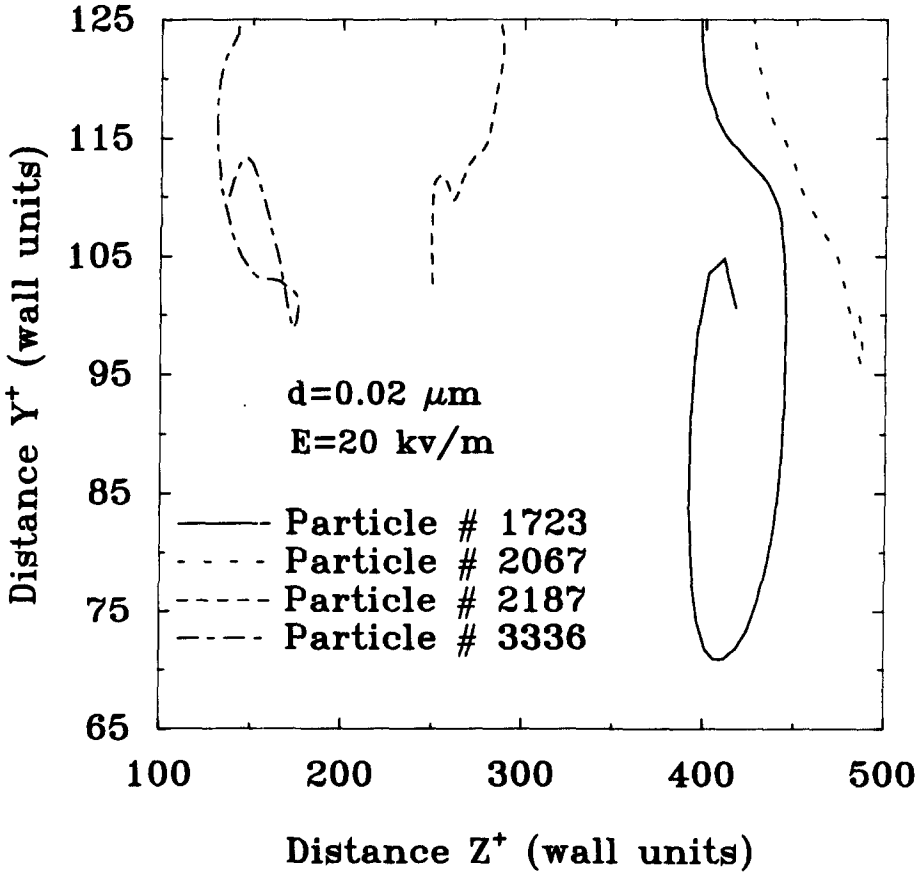

Figure 7. Sample particle trajectories in the yz plane.

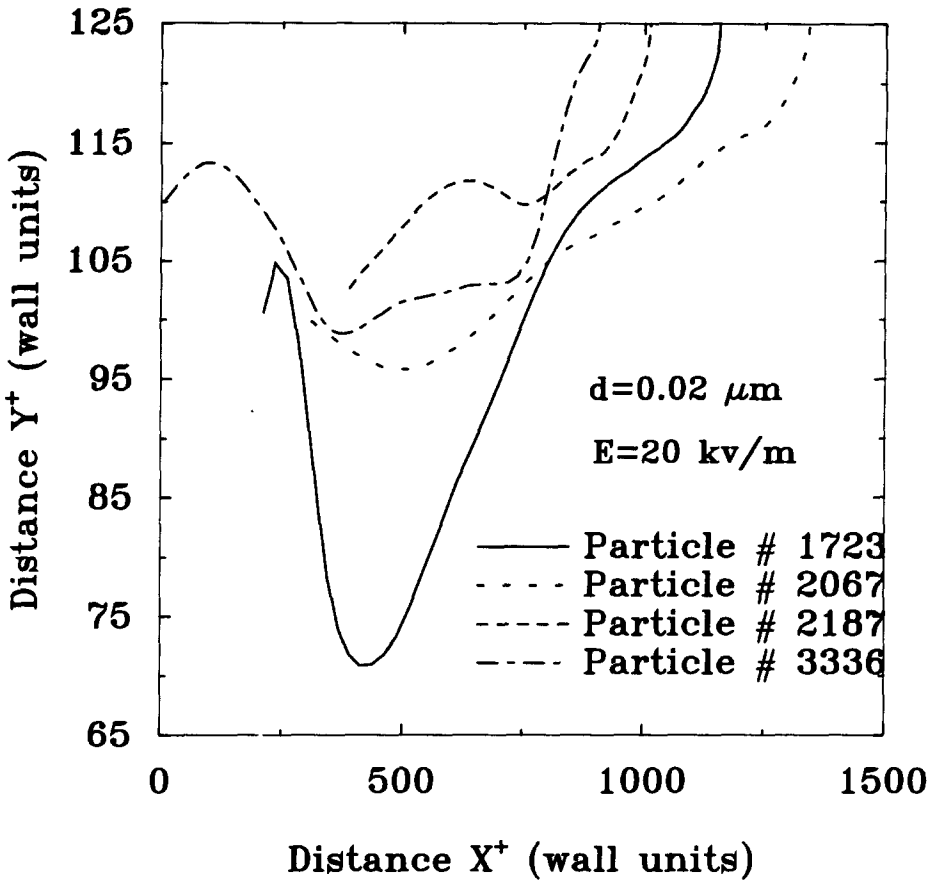

Figure 8. Sample trajectories for charged 0.02 μm particles in the xy plane.

300 μm and electric field strengths of 20 and 200 kV/m are used in these digital simulations. (A particle-to-fluid density ratio of 713 corresponds to olive oil droplets suspended in the air.) For each diameter, ensembles of 8192 particles are uniformly distributed near the wall and a time duration of 100 wall units is used to evaluate the corresponding particle deposition velocity. In the simulations, the particles are initially released with a uniform concentration between 1 and 30 wall units and a linearly varying concentration within one wall unit from the wall. The dimensionless deposition velocity for particles released with a uniform concentration C_0 near a surface is given by

$$u_d^+ = J/C_0 u^* \qquad [23]$$

where J is the particle mass flux to the wall per unit time. The deposition velocity, u_d^+, in [23] may be estimated as

$$u_d^+ = \frac{N_d/t_d^+}{N_0/y_0^+} \qquad [24]$$

where N_0 is the initial number of particles uniformly distributed in a region within an initial distance y_0^+ from the wall, and N_d is the number of deposited particles in the time duration t_d^+. The time interval should be selected in the quasi-equilibrium condition when N_d/t_d^+ remains constant. In the simulations, it is also assumed that once a particle reaches the wall, it sticks to it.

The mean number of charges on all particles was used in most earlier related studies. While this assumption may lead to reasonable results, in certain cases, having a fractional number of charges is physically incorrect. In reality, particles can have either integer number of positive or negative charges or can be neutral. In the present simulations, particles are assigned a random integer

number of charges in accordance with the Boltzmann distribution. In addition, some simulation results for the case that all particles carry the mean number of charge are also presented for comparison.

Figure 2 shows variations of deposition velocity with particle diameter and particle relaxation time for different electrical field strengths. The results for neutral particles are also shown in this figure for comparison. For charged particles, it is assumed that when the particle carries an average charge, the Coulomb force is directed toward the surface. The deposition velocities as given by [21] and [22] are also shown in this figure. It is observed that the deposition rate of small charged particles reaches a peak value for 0.02 to 0.03 μm particles (with nondimensional relaxation time of 10^{-6} to 2×10^{-6} for $u^* = 3.7$ cm/s), and decreases significantly as the particle diameter increases. The reason is that the Coulomb force dominates the particle deposition process in this range. The electrostatic effect decreases as the particle diameter increases. Very few particles smaller than 0.01 μm carry charge, therefore the electrostatic effect decreases in this range. For particles less than 10 μm ($\tau_p^+ < 0.02$), figure 2 also shows that the rate of electrostatic sedimentation increases rapidly as the electric field strength increases. The amount of increase is about 10 times as the field strength changes from 20 to 200 kV/m. For particles greater than 20 to 100 μm, the turbulent eddy-impaction effect becomes important, and the deposition rate increases sharply as the particle diameter increases further. The effect of electrostatic forces becomes secondary for these large particles under a Boltzmann distribution. Figure 2 also shows that the simulated deposition velocities for particles with Boltzmann charge distribution are in close agreement with the predictions of the empirical equations given by [21] and [22].

Sample simulated deposition velocities for particles with uniform charge distribution for an electric field of 20 kV/m are also shown in figure 2. Here, it is assumed that the particles have absolute average charges as given in table 1, half of which are positive and the other half negative.

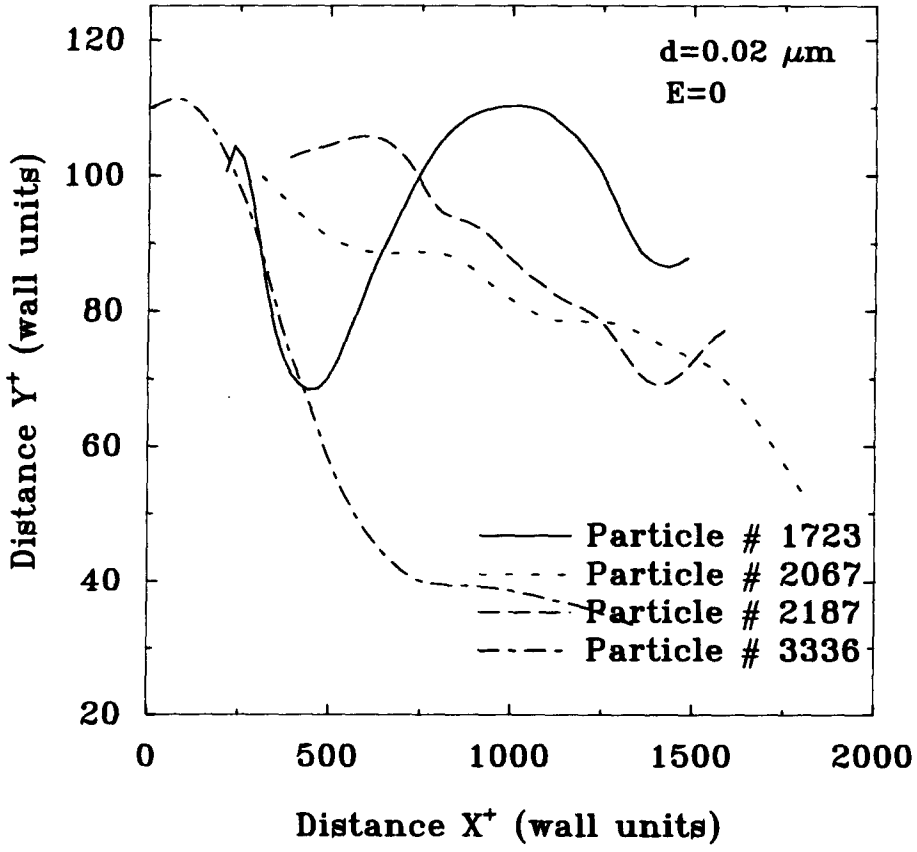

Figure 9. Sample trajectories for neutral 0.02 μm particles in the xy plane.

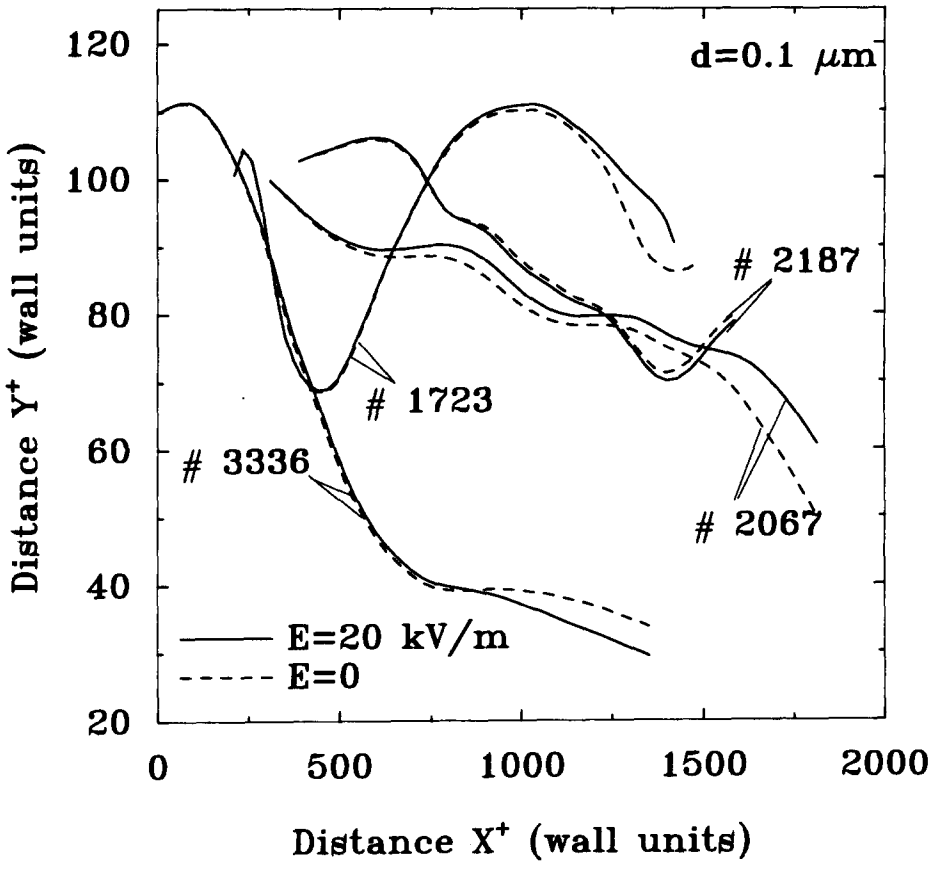

Figure 10. Comparison of sample trajectories for charged and neutral 0.1 μm particles in the xy plane.

It is observed that using the average charge for simulating the effect of electrostatic forces somewhat underestimates the deposition rate. This is due to the fact that the particles acquire integer number of charges which is not necessarily equivalent to the case that all particles carry an average number of charge. It should be emphasized that submicrometer particles with an integer number of charges are strongly affected by the presence of an electric field. This observation is consistent with the earlier results of Li and Ahmadi (1993a, b).

In an earlier work, Ounis *et al.* (1993) have shown that the distribution of the initial locations of deposited (neutral) particles in the plane parallel to the wall form distinct lines. This observation emphasizes further the importance of near wall coherent eddies on the particle deposition process. Here, the effect of electrostatic force on the distribution of the initial locations of deposited particles is studied. The simulation data for particles with the Boltzmann charge distribution is compiled and the initial location of deposited particles in the xz plane is evaluated. The results for 0.02, 2, and 300 μm deposited (charged) particles in the upper half of the channel in the presence of an imposed electric field are shown in figures 3–5. The results for 0.02 μm particles in the absence of electric field are also shown in figure 3 for comparison. For 0.02 and 2 μm particles (with τ_p^+ of 1.17×10^{-6} and 0.001), figures 3 and 4 indicate that the initial location of deposited particles is randomly distributed. The reason is that for submicrometer particles the electrostatic force and Brownian diffusion have a dominating effect on the deposition process. The results for 300 μm particles ($\tau_p^+ = 21.7$) shown in figure 5 indicate that the initial location of the deposited particles is scattered around lines along the channel. These bands correspond to the location of streamwise vortices shown in figure 1. This implies that large particles are mainly deposited by downsweep motions generated by the coherent vortices, and the electrostatic effects (for the Boltzmann charge distribution) are secondary.

To study the effect of electrostatic field on particle trajectories near the wall, several simulations

are performed. Sample trajectories of charged 0.02 μm ($\tau_p^+ = 1.17 \times 10^{-6}$) particles that are deposited in the presence of an electric field of 20 kV/m are displayed in figures 6–8. Figure 6 shows that the particles are transported along the channel in the xz plane. Figures 7 and 8 show the yz and xy projection of particle trajectories. (Note that $y^+ = 125$ is the upper wall in this figure.) The random particle motions due to air turbulence are clearly noticed from these figures. It is also noticed that some particles first move away from the wall before depositing on the wall. This implies that the near wall turbulent flow strongly affects the motion of these submicron charged particles.

The simulations for the particles described in figures 6–8 are repeated in the absence of an electric field. Figure 9 shows the trajectories of neutral 0.02 μm particles in the xy plane. In contrast to the charged ones, these particles are no longer deposited on the wall. This implies that the electrostatic forces play a major role in the deposition of charged 0.02 μm particles in the presence of a 20 kV/m electric field. Figure 9 also shows that the particle number 1723 first moves away from the wall and then moves toward the wall but does not deposit on the wall in the absence of electrical forces.

Comparisons of sample trajectories for charged 0.1 and 300 μm particles in the presence of an electric field with neutral ones are shown in figures 10 and 11. Here, an electric field of 20 kV/m is assumed to be present. It is observed that these particles do not deposit and generally are moving away from the wall. Figure 10 shows that the trajectories of charged and neutral 0.1 μm particles deviate to an extent. This implies that the effects of both electrostatic and turbulence near wall eddies are important for this size of particle. Figure 11 indicates that the trajectories for charged and neutral 300 μm particles are identical. This means the 300 μm particle motions are mainly controlled by the air flow turbulence and the electrostatic effects are secondary. These observations are consistent with the results for deposition velocity shown in figure 2.

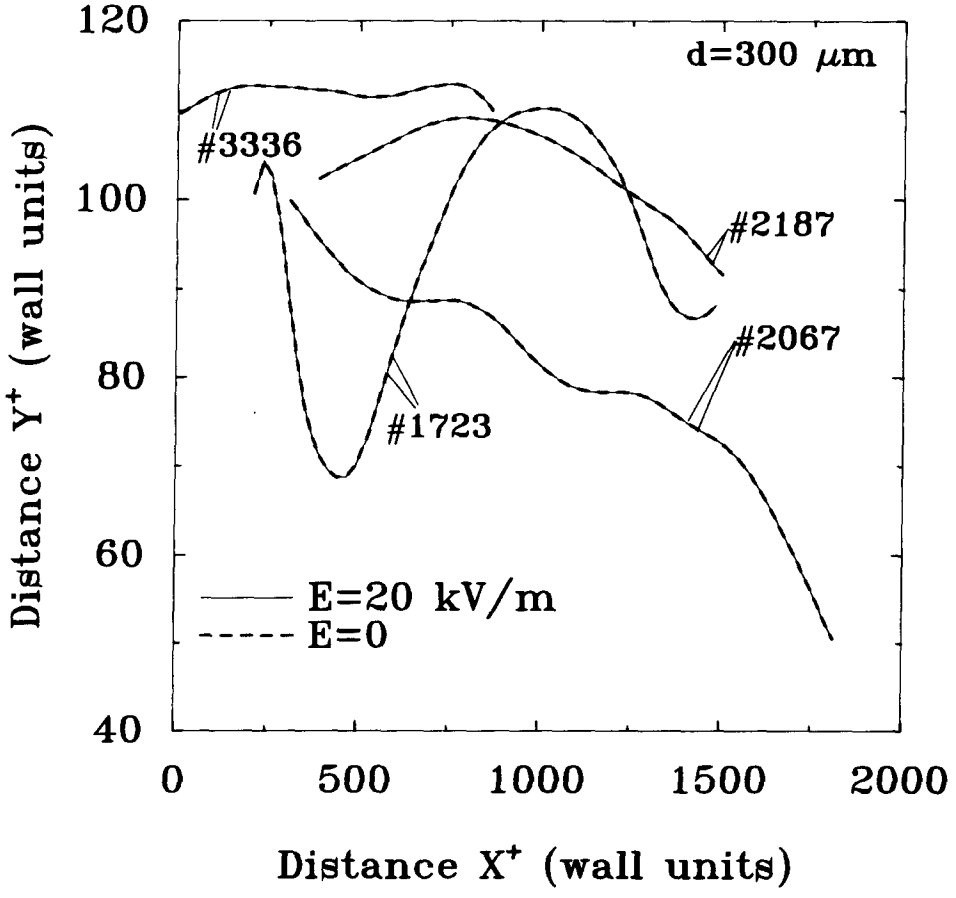

Figure 11. Comparison of sample trajectories for charged and neutral 300 μm particles in the xy plane.

9. CONCLUSIONS

In this work, a digital simulation method for analyzing the deposition rate of charged aerosol particles in a turbulent channel flow in the presence of an applied electric field is described. The particle equation of motion includes the Coulomb and image forces in addition to the Brownian force, the Saffman lift force and turbulent dispersion effects. Starting with an initially uniform concentration near the wall, deposition velocities of charged particles under the Boltzmann equilibrium distribution are evaluated. Deposition rates of particles carrying an average charge are also studied. Several different electric field strengths are considered and the resulting deposition velocities are compared with those obtained from empirical equations. Based on the presented results, the following conclusions may be drawn.

- Electrostatic effects significantly increase the deposition velocity for particles smaller than 20 μm (for $u^* = 3.7$ cm/s, $\tau_p^+ < 0.1$).
- The Boltzmann charge distribution rather than a uniform distribution of mean number of charge must be used in the simulation. Use of a uniform distribution of average charge in the simulation would result in underestimating the deposition velocity.
- The deposition rate of charged particles increases sharply as the electrical field strength increases.
- The deposition velocity of charged particles under the assumption of Boltzmann distribution has a local peak for particle diameter of about 0.02 to 0.03 μm ($\tau_p^+ = 1.17 \times 10^{-6}$ for $u^* = 3.7$ cm/s).
- The Brownian diffusion strongly affects the dispersion of submicron particles near a wall.
- The downsweep streams toward the wall due to the near wall vortices are important for deposition of particles. In particular, the deposition of charged particles with diameter greater than 20 μm ($\tau_p^+ > 0.1$) is strongly affected by the coherent eddies.
- The air flow turbulence affects the particle trajectories (the random particle motions) for particle diameter of 0.02 μm where the maximum deposition rate of particles occurs.
- The present simulation results are in good agreement with the empirical equations.

Acknowledgements—The support of the Department of Energy under Grant DE-FG22-94PC-94213 and the New York State Science and Technology Foundation through the Center for Advanced Material Processing (CAMP) of Clarkson University is gratefully acknowledged. The computer simulation was in part performed at the Cornell National Supercomputer Facilities (CNSF).

REFERENCES

Abuzeid, S., Busnaina, A. A. and Ahmadi, G. (1991) Wall deposition of aerosol particles in a turbulent channel flow. *J. Aerosol Sci.* **22,** 43–62.

Adachi, M., Kousaka, Y. and Okuyama, K. (1985) Unipolar and bipolar diffusion charging of ultrafine aerosol particles. *J. Aerosol Sci.* **16,** 109–123.

Ahmadi, G. (1972) The Brownian motion of charged particles in the presence of a magnetic field. *Iranian J. Sci. Technol.* **1,** 301–310.

Ahmadi, G. and Goldschmidt, V. M. (1971) Motion of particle in a turbulent fluid – the Basset history term. *J. Appl. Mech., Trans. ASME* **38,** 561–563.

Azab, K. A. and McLaughlin, J. B. (1987) Modeling the viscous wall region. *Phys. Fluids* **30,** 2362–2373.

Brooke, J. W., Kontomaris, K., Hanratty, T. J. and McLaughlin, J. B. (1992) Turbulent deposition and trapping of aerosols at a wall. *Phys. Fluids A* **4,** 825–834.

Chen, R. Y. (1978a) Deposition of charged particles in tubes. *J. Aerosol Sci.* **9,** 449–453.

Chen, R. Y. (1978b) Deposition of aerosol particles in a channel due to diffusion and electric charge. *J. Aerosol Sci.* **9,** 253–260.

Cleaver, J. W. and Yates, B. (1975) A sublayer model for the deposition of particles from a turbulent flow. *Chem. Eng. Sci.* **30,** 983–992.

Clift, R., Grace, J. R. and Weber, M. E. (1978) *Bubbles, Drops, and Particles*. Academic Press, New York.

Cooper, D. W., Peters, M. H. and Miller, R. J. (1989) Predicted deposition of submicron particles due to diffusion and electrostatics in viscous axisymmetric stagnation-point flow. *Aerosol Sci. Technol.* **11,** 133–143.

Fan, F.-G. and Ahmadi, G. (1993) A sublayer model for turbulent deposition of particles in vertical ducts with smooth and rough surfaces. *J. Aerosol Sci.* **24,** 45–64.

Fan, F.-G. and Ahmadi, G. (1994) On the sublayer model for turbulent deposition of aerosol particles in the presence of gravity and electric field. *J. Aerosol Sci. Technol.* **21,** 49–71.

Fuchs, N. A. (1964) *The Mechanics of Aerosol*. Pergamon, Oxford.

Hartmann, G. C., Marks, L. M. and Yang, C. C. (1976) Physical models for photoactive pigment electrophotography. *J. Appl. Phys.* **47,** 5409–5420.

Hidy, G. M. (1984) *Aerosols, An Industrial and Environmental Science*. Academic Press, New York.

Li, A. and Ahmadi, G. (1992) Dispersion and deposition of spherical particles from point sources in a turbulent channel flow. *Aerosol Sci. Technol.* **16,** 209–226.

Li, A. and Ahmadi, G. (1993a) Aerosol particles deposition with electrostatic attraction in turbulent channel flow. *J. Colloid Interface Sci.* **158,** 476–482.

Li, A. and Ahmadi, G. (1993b) Computer simulation of deposition of aerosols on surfaces in a turbulent channel flow with rough walls. *Aerosol Sci. Technol.* **18,** 11–24.

Li, A., Ahmadi, G., Bayer, R. G. and Gaynes, A. (1994) Aerosol particle deposition in an obstructed turbulent duct flow. *J. Aerosol Sci.* **25,** 91–112.

McLaughlin, J. B. (1989) Aerosol particle deposition in numerically simulated channel flow. *Phys. Fluids A* **1,** 1211–1224.

McLaughlin, J. B. (1994) Numerical computation of particles turbulence interaction. *Int. J. Multiphase Flow* **20,** 211–232.

Ounis, H. and Ahmadi, G. (1989) Motions of small rigid spheres in a simulated random velocity field. *ASCE J. Eng. Mech.* **115,** 2107–2121.

Ounis, H. and Ahmadi, G. (1990a) Analysis of dispersion of small spherical particles in a random velocity field. *J. Fluid Eng. Trans. ASME* **112,** 114–120.

Ounis, H. and Ahmadi, G. (1990b) A comparison of Brownian and turbulent diffusions. *Aerosol Sci. Technol.* **13,** 47–53.

Ounis, H., Ahmadi, G. and McLaughlin, J. B. (1991a) Dispersion and deposition of Brownian particles from point sources in a simulated turbulent channel flow. *J. Colloid Interface Sci.* **147,** 233–250.

Ounis, H., Ahmadi, G. and McLaughlin, J. B. (1991b) Brownian diffusion of submicron particles in the viscous sublayer. *J. Colloid Interface Sci.* **134,** 497–521.

Ounis, H., Ahmadi, G. and McLaughlin, J. B. (1993) Brownian particle deposition in a directly simulated turbulent channel flow. *Phys. Fluids A* **5,** 1427–1432.

Porstendorfer, J., Hussin, A., Scheibel, H. G. and Becker, K. H. (1984) Bipolar diffusion charging of aerosol particles—II. Influence of the concentration ratio of positive and negative ions on the charge distribution. *J. Aerosol Sci.* **15,** 47–56.

Saffman, P. G. (1968) The lift on a small sphere in a slow shear flow. *J. Fluid Mech.* **31,** 264.

Soldati, A., Andreussi, P. and Banerjee, S. (1993) Direct simulation of turbulent particle transport in electrostatic precipitators. *AIChE J.* **39,** 1910–1919.

Squires, K. D. and Eaton, J. K. (1991) Preferential concentration of particles by turbulence. *Phys. Fluids A* **3,** 1169–1178.

Wood, N. B. (1981) The mass transfer of particles and acid vapor to cooled surfaces. *J. Institute Energy* **76,** 76–93.

Yu, C. P. and Chandra, K. (1978) Deposition of charged particles from laminar flows in rectangular and cylindrical channels by image force. *J. Aerosol Sci.* **9,** 175–180.